

Deep Learning assisted Port-Cycling based Channel Sounding for Precoder Estimation in Massive MIMO Arrays

Advaith Arun, Shiv Shankar, Dhivagar Baskaran, Klutto Milleth, Bhaskar Ramamurthi

Centre of Excellence in Wireless Technology IIT Madras, India

{advaith22, shivshankar, dhivagar.b, klutto}@cewit.org.in

arXiv:2601.14953v1 [eess.SP] 21 Jan 2026

Abstract—Future wireless systems are expected to employ a substantially larger number of transmit ports for channel state information (CSI) estimation compared to current specifications. Although scaling ports improves spectral efficiency, it also increases the resource overhead to transmit reference signals across the time-frequency grid, ultimately reducing achievable data throughput. In this work, we propose a deep learning (DL)-based CSI reconstruction framework that serves as an enabler for reliable CSI acquisition in future 6G systems. The proposed solution involves designing a port-cycling mechanism that sequentially sounds different portions of CSI ports across time, thereby lowering the overhead while preserving channel observability. The proposed CSI Adaptive Network (CsiAdaNet) model exploits the resulting sparse measurements and captures both spatial and temporal correlations to accurately reconstruct the full-port CSI. The simulation results show that our method achieves overhead reduction while maintaining high CSI reconstruction accuracy.

Index Terms—CSI-RS, massive MIMO, 6G, DL, overhead reduction, port cycling, spatial domain reduction, Type-II codebooks.

I. INTRODUCTION

THE massive multiple-input multiple-output (MIMO) system is a key technology for wireless communication systems, offering benefits including spatial multiplexing, capacity gain, etc. To achieve these benefits, accurate CSI is vital, which incurs substantial reference signal overhead with increasing channel dimensions. In current systems, downlink channel acquisition is performed using CSI-RS [1]. It is useful in assessing channel conditions and reports back the channel quality, the number of independent streams, and the beamforming vector to be utilized [2]; however, its overhead grows linearly with the array size thereby reducing the resources available for data transmission.

To address the growing overhead, industry and academic efforts have explored Artificial Intelligence/ Machine Learning (AI/ML) techniques for CSI feedback. In particular, 3GPP has identified AI/ML based CSI compression and prediction as initial use-cases for AI/ML based air interface [3]. From an academic perspective, CsiNet was the pioneer in demonstrating effective non-linear compression of CSI with reduced payload sizes [4]. In [5], authors have investigated CSI extrapolation across time, frequency and spatial domains to actively work on feedback reduction. While these approaches reduce feedback overhead or solve temporal issues, they do not address the instantaneous overhead associated with sounding a large

number of antenna ports, which remains a main bottleneck in massive MIMO systems.

Motivated by this observation, this work focuses on reducing instantaneous channel sounding overhead in the antenna dimension, while maintaining compatibility with current standard compliant transmission. Unlike the environment based channel prediction approach that rely on site-specific information (i.e. images) [6], we adopt a port-cycling based channel sounding strategy in which a subset of ports are activated at a particular time instant, and the full panel is sequentially covered over multiple cycles.

Building on this framework, we propose CsiAdaNet, a deep learning based CSI reconstruction model that exploits the temporal and spatial correlations across the temporally aggregated CSI measurements. By coherently aggregating these sparse observations across time, CsiAdaNet predicts the quantized Type-II precoder defined in 5G NR [1], [7], enabling precoder estimation without requiring full-port instantaneous CSI.

The paper is organized as follows: The system model, port cycling scheme are introduced in Section-II. In Section-III, the details behind the CsiAdaNet model are described. The simulation setup and the results are described in Section-IV. The conclusions are summarized in Section-V.

II. SYSTEM MODEL

Consider a downlink massive MIMO system with $N_t \gg 1$ transmit antennas with a uniform planar array at the base station (BS) and N_r receive antennas at the UE. The system is operated in orthogonal frequency division multiplexing (OFDM) with K subcarriers. The received signal at the k^{th} subcarrier can be expressed as

$$\mathbf{y}_k = \mathbf{h}_k \mathbf{v}_k^H \mathbf{x}_k + \mathbf{n}_k, \quad (1)$$

where $\mathbf{y}_k \in \mathbb{C}^{N_r \times 1}$ denotes the received signal, $\mathbf{h}_k \in \mathbb{C}^{N_r \times N_t}$ denotes the channel matrix, $\mathbf{v}_k \in \mathbb{C}^{N_L \times N_t}$ denotes the precoding vector, $\mathbf{x}_k \in \mathbb{C}^{N_L \times 1}$ denotes the data vector and \mathbf{n}_k denotes the additive noise of the k^{th} subcarrier. The BS is equipped with $N_t = 2 \times N_x \times N_y$ antennas, where N_x, N_y denotes the number of dual polarized antenna elements at the horizontal and vertical dimensions. The channel matrix $\mathcal{H} \in \mathbb{C}^{N_r \times N_t \times K}$ is obtained by stacking the channel matrices of each CSI subcarrier respectively.

A. Type II codebook in 5G NR

5G-NR defines the configurable Type-II of codebooks based on a 2D-DFT based grid of beams in horizontal and vertical dimensions of the antenna array. It selects the optimal L orthogonal beams and linearly combines them in such a way that it maximizes the energy in the eigen vector direction. The Rel.15 Type-II codebook [1] for a given layer ν and the entire wideband is defined as:

$$\mathbf{W}^{(\nu)} = \mathbf{\Lambda}^{(\nu)} \begin{bmatrix} \sum_{i=0}^{L-1} v_{l^{(i)}m^{(i)}} p_{\nu,i} \varphi_{\nu,i} \\ \sum_{i=0}^{L-1} v_{l^{(i)}m^{(i)}} p_{\nu,i+L} \varphi_{\nu,i+L} \end{bmatrix} \quad (2)$$

Quantity	Description
$v_{l,m}$	IDFT beam, $v_{l,m} = v_l \otimes u_m$ v_l : horizontal beam; u_m : vertical beam
L	Number of beams, $L \in \{2, 3, 4\}$
p_ν	Wideband amplitude
φ_ν	Wideband phase
$\Lambda^{(\nu)}$	Normalization factor $\Lambda^{(\nu)} = \frac{1}{\sqrt{N_x N_y \sum_{l=0}^{2L-1} (p_l)^2}}$

TABLE I: Rel.15 Type-II quantities

- **Beam Set:** It refers to the over sampled beam group out of the available $O_1 O_2$ groups.
- **Beam Indices:** It refers to the top- L orthogonal beams out of $N_1 N_2$ beams within the selected beamset.
- **Wideband Amplitude:** It corresponds to reporting the quantized wideband amplitudes for the selected $2L - 1$ orthogonal beams. The strongest beam within the beam set is normalized to unit amplitude. The quantized amplitudes are drawn from the set, $P = \{0, \sqrt{\frac{1}{64}}, \sqrt{\frac{1}{32}}, \sqrt{\frac{1}{16}}, \sqrt{\frac{1}{8}}, \sqrt{\frac{1}{4}}, \sqrt{\frac{1}{2}}, 1\}$
- **Wideband Phase:** This corresponds to the reporting of wideband phase of the selected $2L - 1$ orthogonal beams. The strongest beam within the beam set is normalized to zero phase. The quantized phase alphabets are drawn from the set $\Phi = \{e^{\frac{j2\pi n}{N_{psk}}}, n \in \{0, 1, \dots, N_{psk} - 1\}\}$

The beams are selected from within a beamset based on Algorithm 1 [8] and the wideband components are computed based on Algorithm 2.

B. Sub-array partitioning

The main motivation in this work is to utilize a lesser number of ports for active transmission of reference signals. To reduce the number of active ports for transmission, the full-planar array is partitioned into smaller sub-arrays. In general, the active subset of ports can be selected using sub-panel, interleaved or arbitrary configurations. In this work, we opt to model the sub-array based on sub-panel partitioning, as it preserves the antenna spacing, thereby avoiding spatial aliasing in the beam computation.

The uniform planar array of size $(N_x \times N_y)$ is divided into $\rho = \rho_x \times \rho_y$ contiguous sub-panels, each consisting of $N'_x =$

Algorithm 1 Beam set and Beam Indices Selection

```

1: Input: Over-sampled beam grid  $\{\mathbf{V}_b\}_{b=1}^B$ , covariance
    $\mathbf{R} \in \mathbb{C}^{N_t \times N_t}$ ,  $L$  : Number of beams
2: Output: Beam Set ( $B^*$ ), Beam Indices ( $\mathcal{I}^*$ )
3:
   
$$\mathbf{R} = \begin{bmatrix} \mathbf{R}_{11} & \mathbf{R}_{12} \\ \mathbf{R}_{21} & \mathbf{R}_{22} \end{bmatrix}$$

4: for  $b = 1$  to  $B$  do
5:    $\mathbf{r} \leftarrow \mathbf{V}_b^H (\mathbf{R}_{11} + \mathbf{R}_{22}) \mathbf{V}_b$ 
6:    $\mathbf{s} \leftarrow |\text{diag}(\mathbf{r})|$ 
7:    $\mathcal{I}_b \leftarrow \text{TopL}(\mathbf{s})$ 
8:    $\eta_b \leftarrow \sum_{i \in \mathcal{I}_b} s_i$ 
9: end for
10:  $b^* \leftarrow \arg \max_b \eta_b$  ,  $\mathcal{I}^* \leftarrow \mathcal{I}_{b^*}$ 
11: return  $B^*, \mathcal{I}^*$ 

```

Algorithm 2 Wideband Amplitude and Phase Selection

```

1: Input: Beamset  $b^*$ , beam indices  $\mathcal{I}^*$ , covariance matrix
    $\mathbf{R} \in \mathbb{C}^{N_t \times N_t}$ 
2: Output: Wideband Amplitude ( $\mathcal{P}_\nu^*$ ), Wideband Phase
   ( $\varphi_\nu^*$ )
3:  $(\mathbf{A}, \mathbf{E}) \leftarrow \text{EVD}(\mathbf{R})$ 
4:  $\mathbf{e}_{0,\nu} \leftarrow \mathbf{E}[1:N_t/2, \nu]$ ,  $\mathbf{e}_{1,\nu} \leftarrow \mathbf{E}[N_t/2+1:N_t, \nu]$ 
5: for  $l = 1$  to  $L$  do
6:    $p_{0,l}^\nu \leftarrow \mathbf{e}_{0,\nu}^H \mathbf{v}_l$ ,  $p_{1,l}^\nu \leftarrow \mathbf{e}_{1,\nu}^H \mathbf{v}_l$ 
7: end for
8: for pol  $\in \{0, 1\}$  do
9:    $a_{pol}^\nu \leftarrow |p_{pol}^\nu|$ 
10:   $k_{\nu,pol}^* \leftarrow \arg \max_k a_{k,pol}^\nu$ 
11:   $a_{pol}^\nu \leftarrow a_{pol}^\nu / a_{k^*,pol}^\nu$ 
12:   $\mathbf{A}_{\nu,pol} \leftarrow |\mathbf{a}_{pol}^\nu|$ ,  $\theta_{\nu,pol} \leftarrow \angle \mathbf{a}_{pol}^\nu$ 
13:  for  $l = 1$  to  $L$  do
14:     $\mathcal{A}_{pol,l}^\nu \leftarrow \arg \min_i |P_i - A_{pol,l}^\nu|$ 
15:     $\Theta_{pol,l}^\nu \leftarrow \arg \min_j |\Phi_j - \theta_{pol,l}^\nu|$ 
16:  end for
17: end for
18:  $\mathcal{P}_\nu^* \leftarrow P[\mathcal{A}^\nu]$ ,  $\varphi_\nu^* \leftarrow \Phi[\Theta^\nu]$ 
19: return  $\mathcal{P}_\nu^*, \varphi_\nu^*$ 

```

Algorithm 3 Sub-panel Partitioning

```

1: Input: UPA size  $(N_x, N_y)$ , Number of partitions  $\rho = (\rho_x \times \rho_y)$ 
2: Output: Set of sub-arrays  $\mathcal{S}$ 
3:  $N'_x \leftarrow N_x / \rho_x$ ,  $N'_y \leftarrow N_y / \rho_y$ 
4:  $\mathcal{S} \leftarrow \emptyset$ 
5: for  $i = 0$  to  $\rho_x - 1$  do
6:   for  $j = 0$  to  $\rho_y - 1$  do
7:      $\mathcal{S}_{i,j} \leftarrow \text{antenna elements in rows } [iN'_x : (i+1)N'_x] \text{ and cols } [jN'_y : (j+1)N'_y]$ 
8:      $\mathcal{S} \leftarrow \mathcal{S} \cup \{\mathcal{S}_{i,j}\}$ 
9:   end for
10: end for
11: return  $\mathcal{S}$ 

```

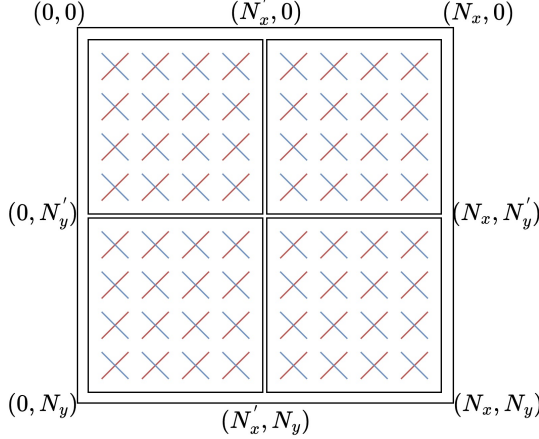


Fig. 1: Illustration of sub-panel based partitioning

N_x/ρ_x and $N'_y = N_y/\rho_y$ antenna elements. This results in ρ non-overlapping sub-arrays, each containing $N'_t = N'_x \times N'_y \times N_{pol}$ ports as mentioned in *Algorithm 3*. and an example configuration is illustrated in Fig. 1.

C. Port Cycling Scheme

It is a method of cycling through the available subset of ports at different time instants for downlink reference signal transmission. The motivation is that, when beam related quantities such as beamset (\mathcal{B}), dominant beam index (\mathcal{I}_0) do not vary across each of the sub-array along time, it underlines the fact that wireless channel statistics such as dominant path, angular spread remain relatively stable within the transmission duration. A score is defined to measure the degree of variation of each of the beam related metric (\mathcal{M}).

$$\text{Variation Score} = \frac{1}{\rho-1} \sum_{i=1}^{\rho-1} |\mathcal{M}^{i+1} - \mathcal{M}^i|.$$

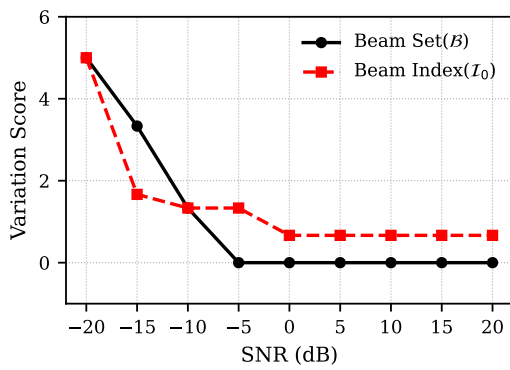


Fig. 2: Plot of variation scores

As shown in Fig. 2, both the beamset index and dominant beam index exhibit low variation across port-cycling instances, particularly at moderate-to-high SNR region. The beamset remains highly stable even under noisy conditions, while the beam index converges quickly with increasing SNR. These

observations validate the feasibility of temporally aggregating port-cycled CSI measurements to predict precoder.

III. CSIADANET

This section provides details about a Deep Learning assisted solution for the port cycling based system. The proposed CSIAdaNet is an DL model that resides at the user equipment (UE) side and operates on ρ periodic CSI measurements, each corresponding to a distinct sub-panel based sub-array with a periodicity of P ms. After cycling through all the ρ sub-panels and estimating the channel corresponding to them, the model predicts the quantized Type-II codebook parameters.

At a given prediction instance, the operation of CsiAdaNet can be expressed as

$$B^*, \mathcal{I}^*, \mathcal{P}^*, \varphi^* = \mathcal{F}(\{\mathcal{H}_{t+iP}\}_{i=0}^{\rho-1}; \theta) \quad (3)$$

where \mathcal{F} denotes the DL model, θ refers to the model parameters and \mathcal{H}_{t+iP} denoting the CSI corresponding to sub-array sounded at time $t + iP$.

The model performs the predictions sequentially with contextual dependency. The beamset is initially predicted, followed by the prediction of the top L beam indices conditioned on the beamset. The predicted beamset and beam indices are then jointly used to estimate the quantized wideband amplitude levels and phase levels, enabling a hierarchical passage of information that remains consistent with the practical codebook selection strategies.

The input to the model consists of ρ sub-array CSI tensors each represented as $\mathcal{H}_t \in \mathbb{R}^{N'_x \times N'_y \times (N_r N_{sc}) \times (2N_{pol})}$, where N'_x, N'_y denote the number of horizontal and vertical antenna elements in the sub-array, N_r is the number of receive antennas, N_{sc} is the number of subcarriers configured for CSI in the entire bandwidth, and $N_{pol} = 2$ denotes the dual polarization. The factor of 2 corresponds to the real and imaginary components of the complex channel co-efficients.

Each CSI tensor is independently processed by a shared encoder module (Enc) to extract the spatial-frequency features. The input is arranged to explicitly preserve the sub-array structure ($N'_x \times N'_y$), enabling the convolutional layers to effectively learn channel variations across the sub-panel dimensions. The encoder consists of three consecutive 3D convolutional layers with filter sizes $\{16, 32, 64\}$ followed by a Global Average Pooling operation to capture the effective features. It is finally passed through a Dense layer of $D = 32$ units, yielding a compact latent representation

$$\mathbf{z}_t = \text{Enc}(\mathcal{H}_t), \mathbf{z}_t \in \mathbb{R}^D \quad (4)$$

To exploit the temporal structure captured by the sequential sub-array sounding, the latent vectors $\{\mathbf{z}_t\}_{t=1}^{\rho}$ are passed through Gated Recurrent Unit (GRU).

The model architecture of CsiAdaNet is illustrated in the Fig. 3, employs multiple heads each corresponding to a distinct CSI feedback quantity. All of the heads operate on a shared latent representation obtained after temporal aggregation from the GRU layers and feature refinement through Head Block units. Each prediction is implemented using a lightweight feed-forward network comprising of a Dense layer followed

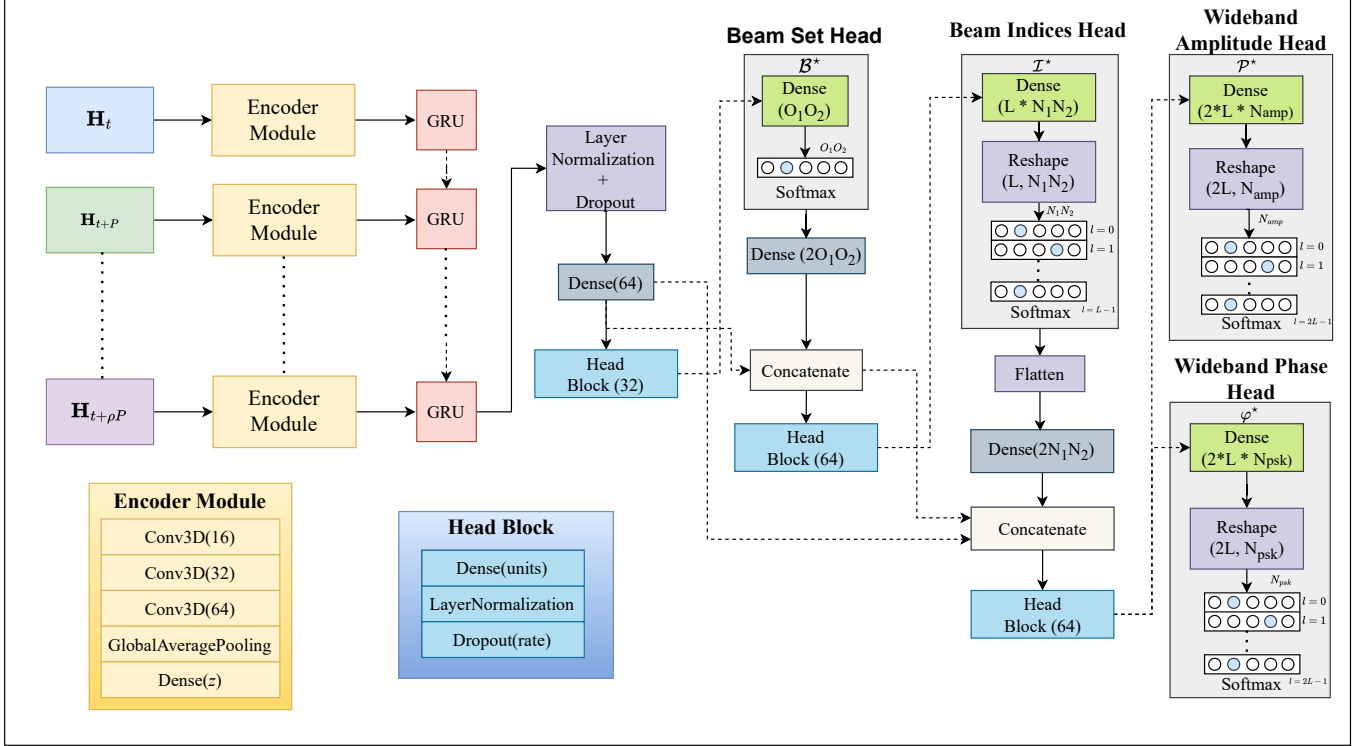


Fig. 3: Model Architecture of CSIAdaNet

by a softmax activation, thereby formulating the outputs as a classification over the respective discrete levels.

Beam Set Head: It predicts the over-sampled beamset index (\mathcal{B}), which is a coarse representation of the spatial direction and rotation in the beam space. The head operates on the shared representation and outputs a probability distribution over the $O_1 \times O_2$ beamset levels.

Beam Indices Head: It predicts the top L beam indices (\mathcal{I}) among the $N_x \times N_y$ orthogonal beams within the selected beamset. It takes in the beamset information in its latent form as an additional information to predict the beam indices accurately.

Wideband Amplitude Head: It predicts the quantized wideband amplitude levels associated with the selected top L beams in the previous stage. The amplitudes capture the power distribution among the selected $2L$ beams and are drawn from a pre-defined finite set P .

Wideband Phase: It predicts the quantized wideband phase levels corresponding to the selected beams. The phase capture a way to coherently combine the selected beams to focus energy in the desired direction. The latent beam information from beamset and beam indices prediction are used in predicting the quantized phase levels.

The CSIAdaNet model is trained using a weighted sum of Sparse-Categorical Cross-Entropy (SCCE) losses for individual CSI quantities. For a single sample, the loss is defined as

$$l_{SCCE}(\hat{x}, p_x) = -\log(p_x[\hat{x}]) \quad (5)$$

where \hat{y} denotes the ground-truth class index and p_x is the predicted class probability score. The task specific loss is given

by

$$\mathcal{L}_x = \mathbb{E}[l_{SCCE}(\hat{x}, p_x)], x \in \{\mathcal{B}, \mathcal{I}, \mathcal{P}, \varphi\} \quad (6)$$

The overall training loss is defined as

$$\mathcal{L}_{total} = \sum_{x \in \{\mathcal{B}, \mathcal{I}, \mathcal{P}, \varphi\}} \lambda_x \mathcal{L}_x \quad (7)$$

The predicted codebook can be reconstructed as

$$\tilde{\mathbf{W}}^{(\nu)} = \mathbf{\Lambda}^{(\nu)} \left[\begin{array}{c} \sum_{i=0}^{L-1} V_b[\mathcal{B}^*][\mathcal{I}_i^*] \times \mathcal{P}_{\nu, i}^* \times e^{j\varphi_{\nu, i}^*} \\ \sum_{i=0}^{L-1} V_b[\mathcal{B}^*][\mathcal{I}_i^*] \times \mathcal{P}_{\nu, i+L}^* \times e^{j\varphi_{\nu, i+L}^*} \end{array} \right] \quad (8)$$

IV. SIMULATION AND RESULTS

In this section, we discuss the simulation framework considered. We use a 3GPP standards compliant proprietary simulator based on 5G NR Rel.19.

A. Link-Level Simulation Assumptions

The simulator is configured to operate on 3GPP Urban Macro (*UMa*) Line-of-Sight (LoS) scenario with an inter-site distance of 200m [9]. It is a single cell setup, sectorized into three sectors. The BS is equipped with 128 antennas in a uniform planar array structure while the UE is configured with 4 antennas. The BS antenna array is partitioned into sub-panel based sub-arrays with spatial domain reduction factor ($\rho = 4$). The periodicity (P) of downlink CSI-RS is set to 20ms. In this simulation, we consider the rank of the channel be to one i.e., $\nu = 1$. The key simulation parameters are summarized in Table II.

Parameter	Value
Deployment Scenario	Urban Macro (UMa) <i>LoS</i>
Number of transmit antennas (N_t)	128
Transmit antenna array configuration	$[N_x = 8, N_y = 8, N_{pol} = 2]$
Number of receive antennas (N_r)	4
CSI-RS periodicity (T_{csi})	20 ms
Carrier frequency (f_c)	3.5 GHz
System bandwidth (BW)	10 MHz
Subcarrier spacing (scs)	15 kHz
UE velocity	30 km/h
Spatial reduction factor (ρ)	4 ($\rho_x = 2, \rho_y = 2$)
Number of antennas per sub-array (N_t')	32

TABLE II: Simulation Assumptions

B. CsiAdaNet Model

The dataset consists of 30,000 samples and is split into training, validation, and test sets in a 70 : 20 : 10 ratio. The model is trained under multiple noise conditions by uniformly applying SNR levels from $\{-5, 0, 5, 10, 15\}$ dB to the training data to increase its robustness. During testing, the model is evaluated independently at each SNR level in $\{-20, -15, -10, -5, 0, 5, 10, 15, 20\}$ dB to assess performance across a wide SNR range. A batch size of 256 is considered for 250 epochs using the Adam optimizer with a learning rate of 10^{-3} . The CsiAdaNet model is trained using a weighted multi-task loss, with a loss weights ($\lambda_B : 0.75, \lambda_I : 1.5, \lambda_P : 0.75, \lambda_\varphi : 1.25$). A higher weightage is assigned to beam indices (λ_I) to emphasize beam selection, as any error in that propagates directly in precoder construction. All of the prediction heads employ sparse categorical cross-entropy losses with sparse categorical accuracy as the evaluation metric. Early stopping is deployed with a patience of 25 and adaptive learning rate reduction are used to stabilize training and avoid overfitting.

To perform prediction, each sub-array is sounded at a different time instant, covering the full array over ρ occasions. During training, all possible sounding orders are to be considered to avoid bias towards a specific sequence; For $\rho = 4$ this results in $4! = 24$ permutations. The port cycled estimates collected over $(\rho \times P)$ ms, forms the input to the DL model, ensuring generalization against sounding order variations.

C. Metrics

As a traditional method, we consider the actual Type-II precoder obtained using the full set of ports (W_{T2}) as the reference for comparison, with the precoder quantities using Algorithms 1 and 2.

Squared Generalized Cosine Similarity(SGCS): It captures the directional alignment between the Type-II precoder traditional or CsiAdaNet predicted, and the dominant eigen vector of the corresponding covariance matrix with the actual number of ports of the channel. It ranges between [0,1].

$$\text{SGCS}(\mathbf{v}_{\text{eig}}, \mathbf{w}) = \frac{|\mathbf{v}_{\text{eig}}^H \mathbf{w}|^2}{\|\mathbf{v}_{\text{eig}}\|_2^2 \|\mathbf{w}\|_2^2}, \mathbf{w} \in [\tilde{W}, W_{T2}] \quad (9)$$

Beamforming Gain (BF): It measures the effective power captured by the Type-II precoder traditional or CsiAdaNet

based, relative to the optimal eigen-beamformer.

$$\text{Gain}(\mathbf{v}_{\mathbf{w},\text{eig}}) = \frac{\mathbf{w}^H \mathbf{R} \mathbf{w}}{\mathbf{v}_{\text{eig}}^H \mathbf{R} \mathbf{v}_{\text{eig}}}, \mathbf{w} \in [\tilde{W}, W_{T2}] \quad (10)$$

where \mathbf{v}_{eig} denotes the dominant eigen vector, \tilde{W} refers to the CsiAdaNet predicted precoder from port-cycled channel measurements and W_{T2} refers to the actual Type-II precoder corresponding to the actual number of ports.

D. Performance Evaluation and Analysis

1) Precoder Alignment and Beamforming Performance:

Figs. 5(a) and 5(b) evaluate the alignment and beamforming performance of the CsiAdaNet predicted precoder. As shown in Fig. 5(a), the DL based approach closely follows the traditional technique in terms of SGCS across all SNR regimes. At low SNR, the SGCS is lower (i.e., < 0.2) due to noise-dominated sub-array CSI, but steadily improves with SNR and saturates at around 0.7 in medium-to-high SNR regime, approaching the baseline trend. Consistently, Fig. 5(b) shows that beamforming gain achieved using CsiAdaNet predicted precoder closely matches the traditional baseline, with a small gap at high SNR (within ≈ 0.03). The drop at low SNR arises from the higher sensitivity of beamforming gain to angular and amplitude estimation errors.

2) Analysis of CSI feedback quantities: Figs. 5(c)–5(f) summarize the prediction accuracy of the individual CSI feedback quantities estimated by CsiAdaNet. In Fig. 5(c), beamset prediction is highly reliable even at moderate SNR levels, which can be attributed to the fact that its a coarse spatial resolution and has inherent robustness to noise and spatial sparsity. This supports the assumption that dominant spatial characteristics remain stable over the port-cycling duration. In Fig. 5(d), the beam indices prediction improves more gradually with SNR, reflecting the increased sensitivity associated with finer angular resolution. The wideband amplitude accuracy in Fig. 5(e) follows a similar trend, as amplitude estimation depends on the correctness of the selected beam indices. Finally, Fig. 5(f) indicates that wideband phase prediction is a challenging task, particularly at low SNR, due to its reliance on coherent combining. Nevertheless, accurate phase estimation is achieved at higher SNR levels, demonstrating the effectiveness of temporally aggregated port-cycled CSI measurements.

3) Complexity Analysis: This subsection compares the computational complexity of the proposed CsiAdaNet model with the conventional covariance based methods. Conventional approaches compute eigenvalue decomposition (EVD) of the full covariance matrix $R_{N_t} \in \mathbb{C}^{N_t \times N_t}$, incurring a complexity of $O(N_t^3)$, along with an additional, $O(O_1 O_2 N_t^2)$ operations for selecting beam related metrics. In contrast, the proposed DL based approach performs inference on sub-panel observations, that scales as a $O(\rho D^2)$, where ρ denotes the number of subpanels and D is the sub-panel feature dimension. The proposed approach remains independent of the full array size N_t , providing improved scalability for large-array systems.

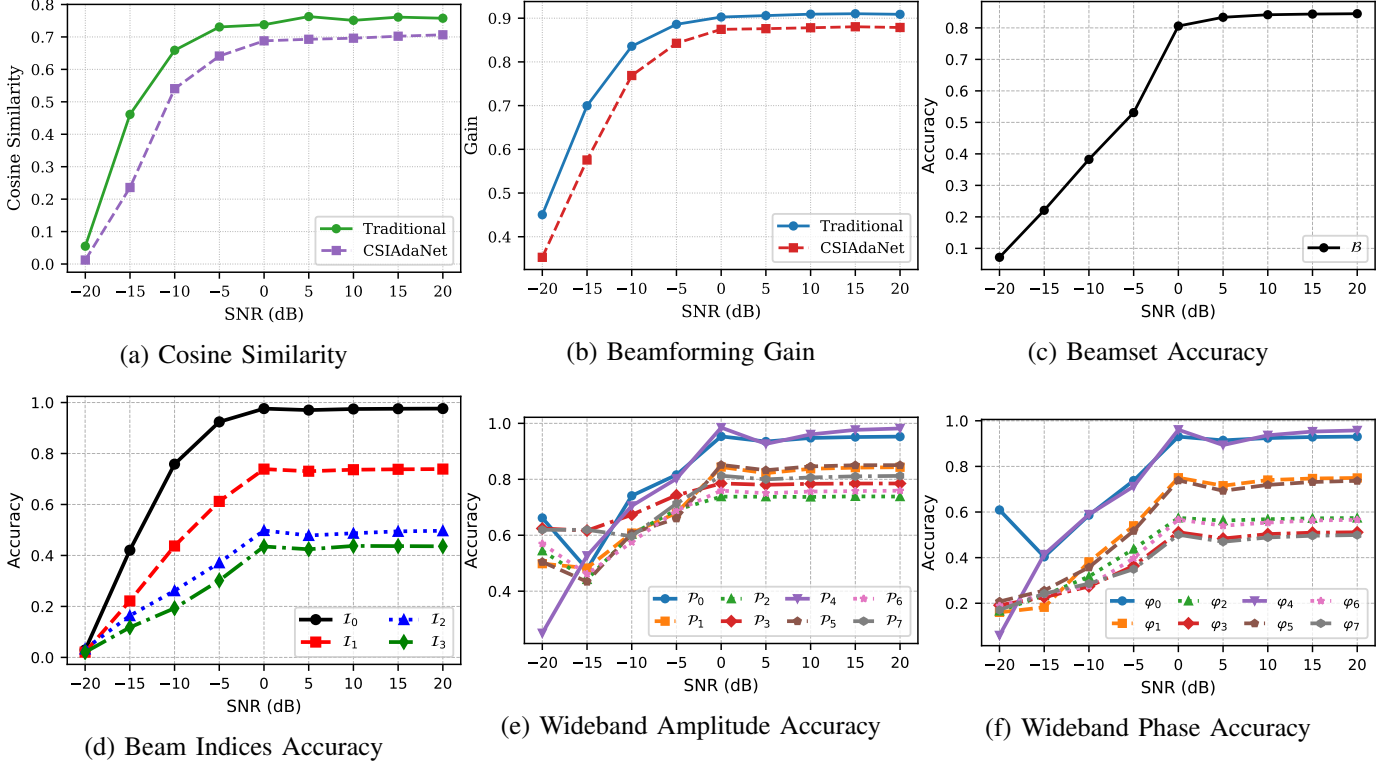


Fig. 4: Performance evaluation of CSI Type-II precoder reconstruction across SNR: (a) cosine similarity, (b) beamforming gain, (c) beamset accuracy, (d) beam indices accuracy, (e) wideband amplitude accuracy, and (f) wideband phase accuracy.

V. CONCLUSION

This work presents a DL-assisted port-cycling based precoder estimation framework that jointly exploits spatial diversity across antennas and temporal diversity enabled by channel stationarity to reduce instantaneous CSI transmission overhead in large MIMO systems. Rather than sounding all ports simultaneously, spatially disjoint sub-panels are activated sequentially, and the resulting partial CSI measurements are coherently aggregated over time. The proposed CsiAdaNet model leverages the resulting spatial-temporal correlations to reconstruct Type-II codebook quantities from reduced CSI observations. Link-level simulations conducted in a 3GPP-compliant setup demonstrate that the proposed approach achieves near-optimal beam alignment and beamforming gain at moderate to high SNR levels, with only marginal degradation under noise-limited regions. Although all antenna ports are eventually sounded across multiple occasions, the number of active ports at any given instant is reduced by a factor of ρ , leading to reduced instantaneous overhead and RF chain utilization. This distinction between instantaneous and aggregate CSI overhead highlights a key design consideration for next-generation large-scale MIMO systems, and demonstrates the effectiveness of exploiting spatial and temporal diversity for scalable and energy-efficient CSI acquisition.

- [1] 3GPP, “Physical layer procedures for data,” 3rd Generation Partnership Project (3GPP), Tech. Rep. TS 38.214, Sep. 2025.
- [2] D. J. Love, R. W. Heath, V. K. N. Lau, D. Gesbert, B. D. Rao, and M. Andrews, “An overview of limited feedback in wireless communication systems,” *IEEE Journal on Selected Areas in Communications*, vol. 26, no. 8, pp. 1341–1365, 2008.
- [3] 3GPP, “Study on AI/ML for NR air interface,” 3rd Generation Partnership Project (3GPP), Tech. Rep. TR 38.843, Jun. 2023.
- [4] C.-K. Wen, W.-T. Shih, and S. Jin, “Deep Learning for Massive MIMO CSI Feedback,” *IEEE Wireless Communications Letters*, vol. 7, no. 5, pp. 748–751, 2018.
- [5] Z. Zhang, J. Zhang, Y. Zhang, L. Yu, and G. Liu, “AI-Based Time, Frequency, and Space-Domain Channel Extrapolation for 6G: Opportunities and Challenges,” *IEEE Vehicular Technology Magazine*, vol. 18, no. 1, pp. 29–39, 2023.
- [6] L. Shi, J. Zhang, L. Yu, Y. Zhang, Z. Zhang, Y. Cai, and G. Liu, “Can Wireless Environment Information Decrease Pilot Overhead: A Channel Prediction Example,” *IEEE Wireless Communications Letters*, vol. 14, no. 3, pp. 861–865, 2025.
- [7] Q. Ziao and Y. Haifan, “A review of codebooks for CSI feedback in 5G new radio and beyond,” *China Communications*, vol. 22, no. 2, pp. 112–127, 2025.
- [8] X. Fu, D. Le Ruyet, R. Visoz, V. Ramireddy, M. Grossmann, M. Landmann, and W. Quiroga, “A Tutorial on Downlink Precoder Selection Strategies for 3GPP MIMO Codebooks,” *IEEE Access*, vol. 11, pp. 138 897–138 922, 2023.
- [9] 3GPP, “Study on channel model for frequencies from 0.5 to 100 GHz,” 3rd Generation Partnership Project (3GPP), Tech. Rep. TR 38.901, Dec. 2019.

REFERENCES

- [1] 3GPP, “Physical layer procedures for data,” 3rd Generation Partnership Project (3GPP), Tech. Rep. TS 38.214, Sep. 2025.